

A Clinically-Grounded Two-Stage Framework for Renal CT Report Generation

Renjie Liang, MSc^a, Zhengkang Fan, MSc^a, Jinqian Pan, MSc^a, Chenkun Sun, MSc^a, Russell Terry, MD^b, Jie Xu, PhD^a,

^a*Department of Health Outcomes and Biomedical Informatics, University of Florida, 2004 Mowry Road, Gainesville, 32611, FL, USA*

^b*Department of Urology, University of Florida, 1600 SW Archer Road, Gainesville, 32611, FL, USA*

Abstract

Generating radiology reports from CT scans remains a complex task due to the nuanced nature of medical imaging and the variability in clinical documentation. In this study, we propose a two-stage framework for generating renal radiology reports from 2D CT slices. First, we extract structured abnormality features using a multi-task learning model trained to identify lesion attributes such as location, size, enhancement, and attenuation. These extracted features are subsequently combined with the corresponding CT image and fed into a fine-tuned vision-language model to generate natural language report sentences aligned with clinical findings. We conduct experiments on a curated dataset of renal CT studies with manually annotated sentence–slice–feature triplets and evaluate performance using both classification metrics and natural language generation metrics. Our results demonstrate that the proposed model outperforms random baselines across all abnormality types, and the generated reports capture key clinical content with reasonable textual accuracy. This exploratory work highlights the feasibility of modular, feature-informed report generation for renal imaging. Future efforts will focus on extending this pipeline to 3D CT volumes and further improving clinical fidelity in multimodal medical AI systems.

1. Introduction

Renal cancer, also known as kidney cancer, is a disease with a rising global incidence, with an estimated 400,000 new cases diagnosed annually and approximately 175,000 deaths worldwide each year [1]. Current projections indicate that the incidence will continue to rise over the next decade, underscoring the urgency of

addressing this growing public health challenge. In the United States alone, more than 81,000 new cases and over 14,000 deaths are expected in 2024 [2]. Although mortality rates have declined by 1–2% annually in recent years due to advances in treatment, the overall incidence continues to increase [2]. The widespread adoption of cross-sectional imaging, particularly computed tomography (CT), has contributed to an increase in the incidental detection of early-stage renal tumors [3]. Early diagnosis is critical, as renal cancer often remains asymptomatic in its initial stages but can progress rapidly if left untreated. Accurate and timely interpretation of renal CT scans is essential for clinical decision-making, including diagnosis, staging, and treatment planning. However, increasing imaging volumes and inter-observer variability pose challenges for radiologists. As such, the development of intelligent systems to support or automate report generation from renal CT images holds significant potential to enhance diagnostic efficiency, reduce variability, and ultimately improve patient care.

Recent years have witnessed remarkable progress in large model technologies, particularly in the development of large language models (LLMs) and vision-language models (VLMs). These foundation models have brought transformative advances across many domains, including biomedical informatics and computer-aided diagnosis. Models such as GPT-4, PaLM, and Med-PaLM have demonstrated the ability to understand clinical narratives, answer medical questions, and even provide diagnostic suggestions, acting as virtual clinical assistants in various scenarios [4, 5, 6]. Similarly, vision-language models such as BioViL and LLaVA-Med integrate visual and textual modalities to support medical image interpretation, question answering, and image-report alignment [7, 8].

These technological breakthroughs have led to a surge of interest in medical imaging applications, particularly in automating radiology workflows. One rapidly growing area is radiology report generation, where deep models learn to produce textual reports directly from medical images. Most existing work in this space has focused on chest X-rays, leveraging large-scale public datasets such as MIMIC-CXR [9] and CheXpert [10], and achieving promising results through image captioning, retrieval-augmented generation, and transformer-based encoder-decoder frameworks [11].

However, relatively little attention has been paid to radiology report generation for other anatomical regions. In particular, there is a lack of work focusing on renal imaging. Existing studies on kidney CT or MRI mainly emphasize classification tasks, such as tumor detection or subtype prediction [12, 13, 14, 15], rather than comprehensive report generation. This gap is partly due to several challenges unique to renal radiology.

First, there is a scarcity of large-scale, publicly available renal CT datasets with paired expert reports, which limits the development and benchmarking of generative models in this domain. Second, unlike chest imaging, there is no widely accepted or standardized reporting template for renal CT scans, especially in the context of renal cancer, making the target output space more diverse and ambiguous. Third, evaluating the quality of generated radiology reports remains a fundamental challenge. Traditional natural language processing (NLP) metrics such as BLEU, ROUGE, and METEOR focus on surface-level lexical overlap and fail to capture clinically critical information. In medical contexts, a single word or numerical value can determine the diagnostic conclusion, meaning that minor errors may have major clinical implications [16].

In this work, we aim to bridge this gap by exploring the feasibility of automated renal radiology report generation. We collect real-world clinical data from the University of Florida (UF) Health System, and, guided by expert radiologists and nephrologists, construct a structured reporting schema tailored for renal imaging. We propose a two-step generation pipeline: the first stage detects key radiological features from 2D CT slices, and the second stage integrates these findings to generate coherent and clinically meaningful textual reports. To the best of our knowledge, this study represents one of the first systematic efforts toward generative modeling in kidney imaging, and lays foundational work for future kidney-specific AI applications in radiology.

2. Statement of Significance

Problem

Radiology report generation has primarily focused on chest X-rays and high-level classification tasks, with limited exploration of generating structured reports for renal cancer using CT slices.

What is Already Known

Recent advancements in computer vision (CV) and large language models (LLMs) have enabled vision-language models (VLMs) to support a wide range of medical imaging tasks, including radiology report generation. These systems have demonstrated success in generating descriptive reports for chest X-rays. However, to date, no system has been specifically designed to generate reports for renal imaging, particularly in the context of kidney cancer.

What This Paper Adds

We present the first system for renal CT report generation using a two-stage pipeline. Based on real-world UF Health data, our method extracts abnormality features and generates clinically meaningful reports.

Who Would Benefit from the New Knowledge in This Paper

AI researchers can leverage this work as a foundation for extending radiology report generation to less-explored anatomical regions. Radiologists and nephrologists may benefit from improved report standardization, enhanced diagnostic support, and reduced manual workload in renal cancer care.

3. Related Work

3.1. Renal Abnormality Diagnosis

Several studies have demonstrated the effectiveness of deep learning approaches in diagnosis kidney abnormalities from CT scans. Alzu’bi et al. [12] proposed a method for classifying renal tumors, cysts, and stones from 2D CT slices using a new dataset. Similarly, Islam et al. [13] developed vision transformer and transfer learning models to differentiate between normal kidneys and those with tumors, cysts, or stones, also based on 2D CT images. Yildirim et al. [15] focused specifically on the detection of kidney stones using coronal CT slices, employing a deep learning architecture for automatic identification. Uhm et al. [14] addressed a more complex diagnostic task by classifying kidney cancer into five subtypes using multi-phase 3D CT scans.

Although these methods demonstrate promising diagnostic capabilities, they primarily focus on generating high-level classification results. None of these works provide a detailed characterization of abnormality features or generate comprehensive radiology reports that mimic clinical narratives. Our work aims to bridge this gap by incorporating structured abnormality features and producing interpretable, report-style outputs.

3.2. Large Language Models

Large language models (LLMs) have demonstrated remarkable capabilities in natural language understanding and generation, leading to growing interest in their application to biomedical domains. OpenAI’s GPT-4 has been shown to perform competitively on medical licensing exams and clinical question-answering tasks [17]. Similarly, Meta’s LLaMA series, particularly LLaMA-2 and its derivatives such as

MedLLaMA, have been adapted for biomedical tasks through domain-specific pre-training or instruction tuning [18]. Qwen, a large-scale Chinese open-source foundation model developed by Alibaba, has also released variants with capabilities in medical understanding, contributing to the multilingual extension of biomedical LLMs [19]. Beyond general-purpose LLMs, several models have been tailored for health-care, such as BioGPT [20], trained on PubMed abstracts, and PMC-LLaMA [21], which combines biomedical knowledge with LLaMA’s architecture. These models have been applied to tasks including medical report summarization, entity extraction, and clinical question answering. However, their use in radiology report generation—particularly for complex imaging modalities such as CT scans—remains limited and underexplored.

3.3. Radiology Report Generation

Radiology report generation has been extensively studied in the context of chest X-ray imaging. Two widely used datasets in this domain are MIMIC-CXR [9] and IU X-Ray [22], both of which provide paired 2D chest X-ray images (including at least posteroanterior and lateral views) and corresponding free-text reports. However, these datasets lack detailed annotations of abnormality features, which limits their utility for structured or explainable report generation. Hamamci et al. [23] introduced a large-scale 3D chest CT dataset that supports multiple tasks, including relevant case retrieval, multi-abnormality detection, and radiology report generation. In a different domain, Lei et al. [24] released a brain MRI dataset that contains both segmentation masks of abnormal regions and manually written radiology reports, enabling grounded report generation with spatial correspondence between images and text.

To the best of our knowledge, our work is the first to focus on radiology report generation for renal imaging. We aim to provide a detailed characterization of abnormality features along with free-text reports, using 2D CT slices of the kidney.

4. Material and Method

4.1. Participants

This study was conducted in compliance with the Declaration of Helsinki, and the requirement for informed written consent was waived by the Institutional Review Board (IRB approval number: IRB202100401). The data used in this study were obtained from the UF Integrated Data Repository, which contains CT scans and

clinical reports from multiple hospitals within the UF Health system.¹

Participants were identified through a multi-stage filtering process based on narrative radiology reports and corresponding CT scans. First, all available reports were extracted and filtered using renal-related CPT-9 codes (74160, 74170, 74175, 74177, 74178), which represent abdominal and pelvic CT scans performed with or without intravenous contrast. Reports matching these codes were considered to be associated with renal imaging. Next, these reports were matched to corresponding CT scan records. Reports that could not be linked to an existing CT study or whose scan data were unavailable were excluded. Among the remaining report–scan pairs, we selected those that explicitly referenced a specific CT slice, typically in the coronal view.

Some reports included multiple references to distinct image slices, each describing a separate abnormality; therefore, a single report could yield multiple annotations. These slice-referenced reports were manually annotated, resulting in 155 annotations from 129 reports. After excluding cases with no reported abnormalities, missing CT series, or CT slices in non-coronal views, we obtained a curated annotation set consisting of 130 annotations from 108 reports across 97 patients. Table 1 summarizes the patient demographics and lesion characteristics of the final cohort. Notably, there is a discrepancy in the distribution of diagnosis labels between the patient-level and lesion-level summaries. The diagnosis labels in the patient demographics are derived from all recorded ICD codes across a patient’s medical history, whereas the lesion-level labels are limited to findings explicitly referenced by a CT slice within the radiology report. As a result, certain diagnoses may be present at the patient level but absent from the lesion-level annotations.

4.2. Data Preprocessing

Our dataset consists of radiology reports, structured renal feature labels, and corresponding CT image slices. The overall preprocessing pipeline is illustrated in Figure 2.

4.2.1. Report

The original radiology reports contain sections such as clinical history, exam details, and findings across multiple organs. For this study, we focused exclusively on renal-related findings that describe CT-based observations. Because our analysis is based on 2D CT slices, we extracted only sentences that explicitly reference specific CT slice locations (e.g., “image 45 series 4”). These sentences were identified using

¹<https://idr.ufhealth.org/>

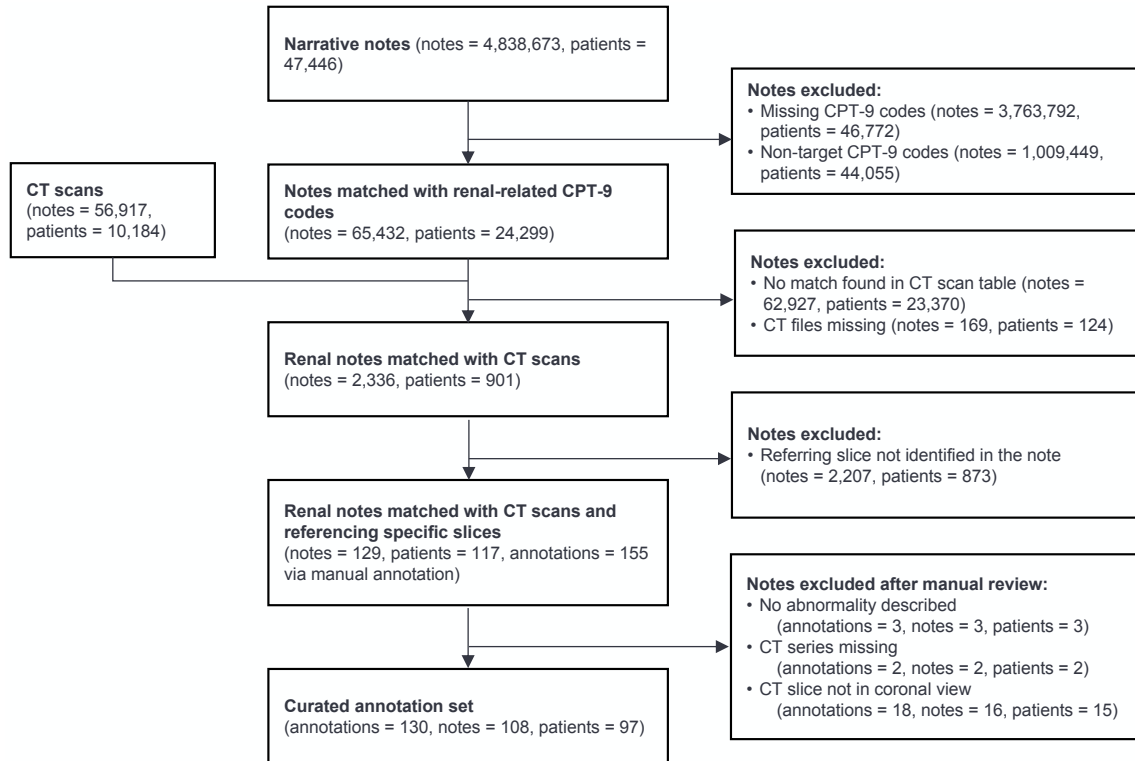


Figure 1: Workflow for filtering and annotating renal CT reports and scans. Reports were filtered based on renal-related CPT-9 codes, scan availability, and explicit slice-level references. Reports referencing non-coronal slices or lacking abnormalities were excluded. Some reports contained multiple slice references, resulting in 130 manual annotations from 97 patients.

Table 1: Summary of Patient and Lesion Characteristics

| Patient Demographics (n = 97) | | Lesion Characteristics (n = 130) | |
|--------------------------------------|--------------|---|--------------|
| Attribute | Value | Attribute | Value |
| Age (years) | 71.56 ± 6.34 | Location | |
| Race | | Right kidney | 68 |
| Black | 30 | Left kidney | 61 |
| White | 66 | Unknown | 1 |
| Other | 1 | Lesion Size (cm) | 1.71 ± 1.20 |
| Ethnicity | | Known cases | 112 |
| Not Hispanic | 96 | Unknown | 18 |
| Unknown | 1 | Growth Pattern | |
| Gender | | Exophytic | 26 |
| Female | 51 | Endophytic | 2 |
| Male | 46 | Unknown | 102 |
| Nephrectomy | | Attenuation | |
| Performed | 7 | Hypoattenuating | 43 |
| Not Performed | 90 | Hyperattenuating | 30 |
| Diagnosis Labels | | Isoattenuating | 6 |
| Cancer | 16 | Unknown | 51 |
| Tumor | 11 | Enhancement | |
| Cyst | 88 | Enhancement | 26 |
| Other | 79 | Non-enhancement | 10 |
| CT Scan Counts | | Unknown | 94 |
| One scan | 69 | Cyst | |
| Two scans | 23 | Present | 78 |
| Three scans | 5 | Absent | 52 |
| | | Mass | |
| | | Present | 15 |
| | | Absent | 115 |
| | | Tumor | |
| | | Present | 7 |
| | | Absent | 123 |

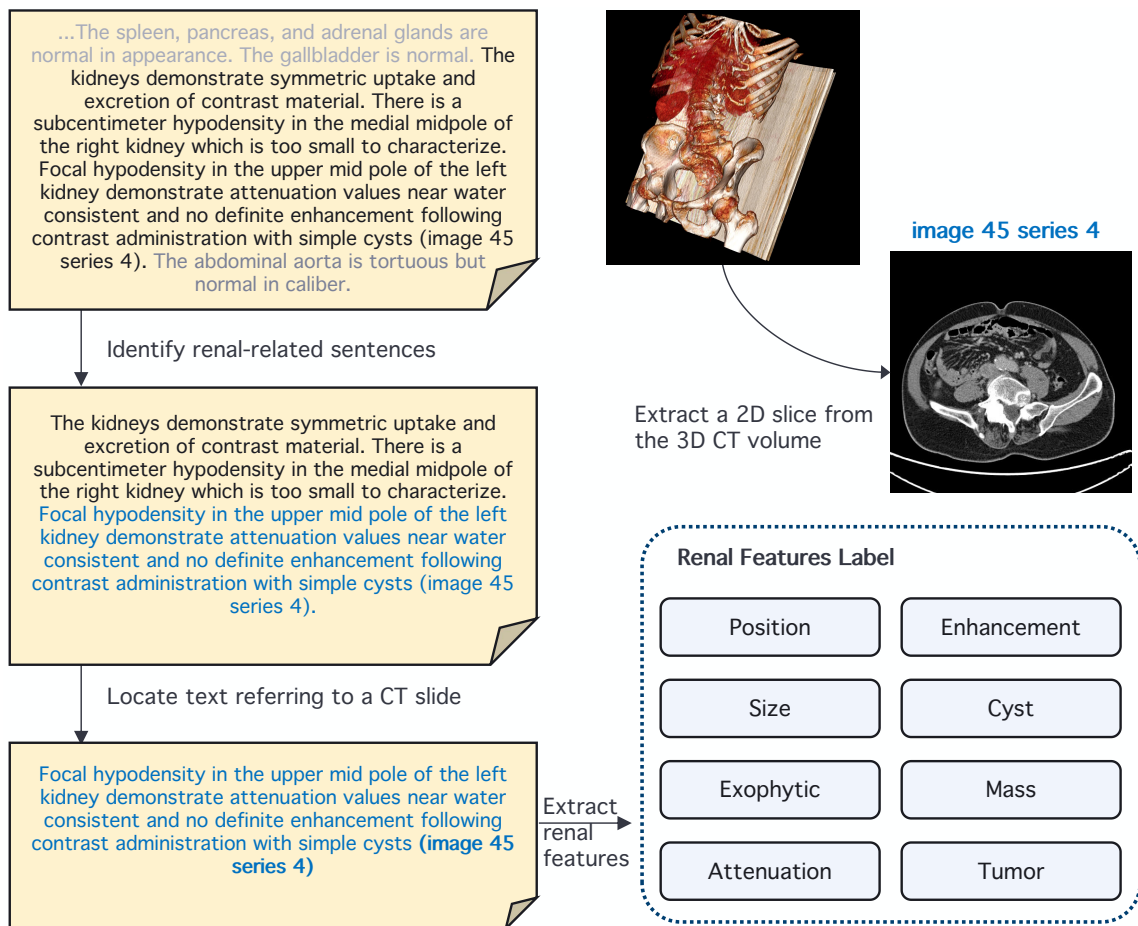


Figure 2: Data preprocessing pipeline. The pipeline includes three main components: (1) identifying renal-related sentences from the medical report; (2) extracting corresponding renal features; and (3) locating and extracting the 2D CT slice that matches the referenced image series in the report.

the Qwen 2.5 large language model [25] with a tailored prompt, followed by manual review to ensure accuracy and completeness. Sentences without explicit image references were excluded, even if they contained potentially relevant renal content. We also excluded slice-referenced sentences describing findings unrelated to renal cancer progression (e.g., nephrolithiasis or hydronephrosis). This filtering ensured that each retained sentence could be aligned with a specific CT slice and remained within the clinical scope of renal cancer. However, this also limited the diversity of renal pathologies represented in the dataset. The prompt used for sentence extraction is provided in Appendix Appendix A.

4.2.2. Feature Labels

Based on guidance from renal specialists and reference materials such as the Radiology Assistant [26] and RadReport [27], we extracted eight renal feature labels: position, size, exophytic, attenuation, enhancement, cyst, mass, and tumor. We followed the annotation schema from [19], using a large language model to extract and structure these labels, followed by manual verification. In cases where the lesion type (cyst, mass, or tumor) could not be directly determined from the report, nephrology experts assisted in the inference. When certain features were not explicitly mentioned in the report, the corresponding feature labels were marked as **Unknown**. For qualitative size descriptions such as “subcentimeter,” we standardized the value to 0.5 cm to ensure consistent numerical representation across the dataset. Many feature categories—particularly growth pattern and enhancement—were frequently unreported in the original reports, resulting in a substantial number of **Unknown** entries (see Table 1). We chose not to impute or assign default values, as omission in clinical documentation does not imply absence. Preserving this missingness reflects the inherent ambiguity of real-world reports and ensures that downstream models are trained and evaluated under realistic, incomplete conditions. The full prompt used for feature label extraction is provided in Appendix Appendix A.

4.2.3. CT Slice

From the 3D CT volumes, we extracted 2D slices explicitly referenced in the radiology reports (e.g., “image 45 series 4”). Slice positions were determined by sorting the DICOM series using the `SliceLocation` attribute, followed by index-based matching to the reported image number. Each slice was then aligned with its corresponding sentence and renal feature labels to form complete data triplets (report sentence, label, CT slice). For detection models, we retained the original Hounsfield Unit (HU) values and deferred augmentation to the training stage, treating augmentation parameters as part of the hyperparameter search. For generative models, we applied fixed windowing (window width = 400, window level = 50) and converted

the slices to PNG format. All CT slices were manually reviewed to ensure they corresponded to the renal region. Slices that were misreferenced or misaligned by the radiologist were excluded to ensure high-quality inputs for downstream modeling.

4.3. Data Splitting and Label Balance

We adopted a 5-fold cross-validation strategy to ensure robustness and generalizability. Data splitting was performed at the annotation level, where each sample corresponds to a unique triplet of (report sentence, label, CT slice). This approach enables stratification across a larger number of samples while preserving label diversity within each fold. To mitigate sampling bias, we applied stratified sampling [28, 29] based on renal feature distributions. For highly imbalanced features—such as the “Exophytic” category, which included only one “endophytic” case—we manually ensured that the minority class was represented in both training and validation sets. The detailed label distribution for one representative fold is provided in Appendix Appendix B.

4.4. Model

To align with the radiology workflow and enhance clinical interpretability, we adopt a two-stage modeling pipeline (Figure 3). In the first stage, we extract renal abnormality features from 2D CT slices using tailored computer vision models. In the second stage, these features—along with the corresponding slice—are fed into a fine-tuned vision-language model (VLM) to generate a free-text report sentence. This modular structure enables both structured feature evaluation and flexible language generation.

4.4.1. Feature Extraction Model

We use a ResNet-34 backbone [30] as the base encoder for CT slice-level feature extraction. Each renal feature label is treated as a separate task:

- Binary classification: Position, Enhancement, Cyst, Mass
- Multi-class classification: Attenuation (hypo-, hyper-, iso-attenuating)
- Regression: Size (cm)
- Anomaly detection: Tumor, Exophytic

The Exophytic and Tumor categories are extremely imbalanced in our dataset (e.g., only one endophytic case among 130 lesions), rendering supervised classification ineffective. For these categories, we employ anomaly detection techniques [31] trained exclusively on negative examples. All models are trained and evaluated using stratified 5-fold cross-validation (Section 4.3), with task-appropriate metrics such as AUROC, MAE, and F1 score.

4.4.2. Report Generation Model

We fine-tune Qwen-VL 2.5 [19], a vision-language model capable of interpreting paired image–text inputs. The generation prompt consists of two components: (1) a structured feature template populated with predicted renal feature labels, and (2) the corresponding CT slice. Together, these inputs are used to generate a radiology report sentence aligned with the annotated source. Model fine-tuning is performed using LLAMA-Factory [32] with instruction-style supervision. For each training sample, the input includes the structured prompt and CT slice, and the target is the expert-written report sentence. Prompt templates used for report generation are provided in Appendix Appendix A.

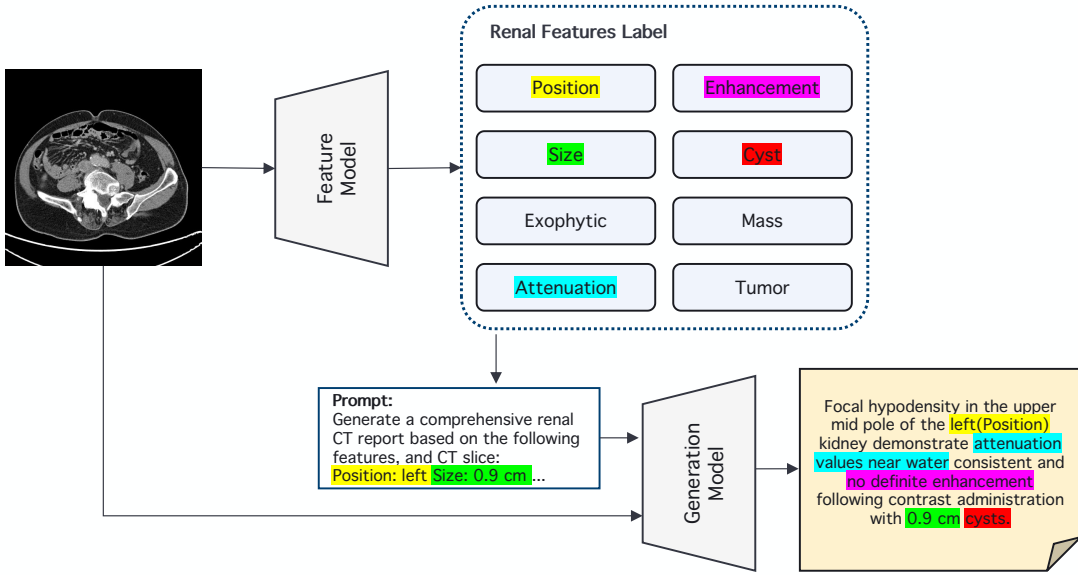


Figure 3: Overview of our two-stage pipeline for renal CT report generation. The Feature Extraction Model identifies structured renal feature labels from 2D CT slices, which are then used by the Report Generation Model to produce the final radiology report sentence.

4.5. Data Augmentation

To improve model robustness and leverage spatial continuity in CT volumes, we applied augmentation strategies inspired by prior work [12]. Specifically, for each annotated 2D CT slice, we included its adjacent slices at offsets of -1 and $+1$, effectively tripling the training data and introducing slight anatomical variation without altering the underlying pathology. This augmentation was applied exclusively to the feature extraction model, and not to the report generation model, as the latter operates on individual CT slices with precise spatial references. We also standardized the

spatial resolution of all CT slices by resizing each to a fixed dimension of 512×512 pixels. For slices larger than this size, we applied center cropping; for smaller ones, we padded the surrounding region with zeros. This resizing strategy ensured consistency across inputs while preserving lesion scale and spatial integrity—particularly important for size-sensitive tasks.

In addition to spatial normalization, we applied standard intensity preprocessing. Raw CT scans were stored in Hounsfield Units (HU), spanning a wide dynamic range that includes soft tissue, bone, and air. To suppress irrelevant structures and emphasize renal parenchyma and lesions, we clipped HU values to a fixed window (window width = 400, window level = 50), as is standard in abdominal imaging. This was followed by min–max normalization to rescale intensity values to the range $[-1, 1]$, promoting training stability and improving convergence.

4.6. Metrics

4.6.1. Feature Extraction Evaluation

To evaluate the performance of the feature extraction model, we adopt standard metrics tailored to each task type. For classification tasks—such as detecting cysts, masses, or tumors—we report Accuracy, Precision, Recall, and F1-score. To account for class imbalance (e.g., the tumor class has very few positive samples), we additionally report the Area Under the Receiver Operating Characteristic Curve (AUC-ROC), which offers a more reliable measure of discriminatory performance in imbalanced scenarios. For regression tasks, such as predicting lesion size, we use Mean Squared Error (MSE) to quantify the average deviation between the predicted and ground truth sizes (in cm). This metric captures both systematic and random errors in continuous predictions.

4.6.2. Report Generation Evaluation

To assess the quality of the generated radiology report sentences, we report standard Natural Language Generation (NLG) metrics including BLEU-4 [33], ROUGE-1, ROUGE-2, and ROUGE-L [34]. These metrics capture n-gram overlap and longest common subsequence between the generated and reference sentences, providing a lexical-level assessment of fluency and content similarity.

5. Results

5.1. Implementation Details

For the clinical feature prediction tasks, we performed grid search over multiple ResNet variants (ResNet-18, ResNet-50, and ResNet-101), initialized with ImageNet-pretrained weights. The input images were preprocessed using the augmentation

strategies described in Section 4.5, including adjacent slice incorporation, intensity clipping, normalization, and resizing to 512×512 resolution. Training was conducted with a batch size of 16, a learning rate of $1e-4$, and the Adam optimizer.

We fine-tuned the Qwen2.5-VL-7B-Instruct model using LoRA (rank = 8) with the LLaMA-Factory framework. CT slices were preprocessed with fixed windowing (level = 50, width = 400) and resized to 512×512 pixels. Structured features were embedded into the prompt alongside the CT image (Appendix Appendix A). Training used a learning rate of $1e-4$, batch size of 4 (with gradient accumulation = 8), and a cosine scheduler over 200 epochs. Mixed-precision training (bf16) was enabled, and evaluation was performed every 50 steps.

All experiments were conducted on a single NVIDIA H100 B200 GPU with 192 GB of memory. Code was implemented in PyTorch 2.2 and Hugging Face Transformers, with all random seeds fixed for reproducibility.

5.2. Feature Extraction Results

Table 2 summarizes the performance of our proposed feature extraction model compared to a random baseline across all annotated abnormality types.

The proposed model substantially outperforms the random baseline across all abnormality detection tasks, indicating reliable learning behavior and good generalization performance. For most binary features—such as *Position*, *Cyst*, and *Tumor*—the model achieved substantial improvements in AUC (e.g., 0.7063 vs. 0.3168 for *Tumor*) and F1-score (0.7400 vs. 0.3510), indicating accurate identification of clinically relevant findings. Particularly strong performance was observed for the *Enhancement* (F1 = 0.8859) and *Tumor* (F1 = 0.7400) categories, which are clinically important for lesion characterization and cancer diagnosis, respectively.

For the multi-class task of *Attenuation*, the model yielded moderate results, with a precision of 0.6300 and F1-score of 0.6167. This is likely due to overlapping Hounsfield Unit (HU) values among hypo-, iso-, and hyperattenuating tissues, as well as the limited availability of explicit attenuation descriptions in the source reports. Nevertheless, the model still achieved more than a twofold improvement in accuracy over the baseline (0.6827 vs. 0.3202), suggesting its ability to learn meaningful attenuation cues.

The evaluation results for the *Exophytic* label appear perfect, but are misleading. Since the dataset contains only a single instance labeled as “endophytic,” which appears in both the training and validation sets, the model likely memorizes this case. As a result, the reported performance does not reflect the true generalization ability for this feature.

For lesion size estimation, the model yielded an overall MSE of 0.9959 cm. Although this value may appear relatively high, further analysis revealed that the performance drop was primarily driven by a single cross-validation fold, in which the validation set contained several large lesions that were underrepresented in the corresponding training set. In other folds, the model demonstrated strong consistency and accuracy, suggesting that adequate size diversity in the training data can substantially enhance regression performance.

Table 2: Comparison of Model Performance Across Abnormality Features

| Feature | Model | AUC | Accuracy | Precision | Recall | F1 / MSE |
|-------------|----------|---------------|---------------|---------------|---------------|---------------|
| Position | Random | 0.4643 | 0.4618 | 0.4539 | 0.4603 | 0.4471 |
| | Proposed | 0.6664 | 0.7166 | 0.7159 | 0.7076 | 0.7050 |
| Exophytic | Random | 0.5043 | 0.4533 | 0.4217 | 0.3471 | 0.3500 |
| | Proposed | 1.0000 | 1.0000 | 1.0000 | 1.0000 | 1.0000 |
| Attenuation | Random | – | 0.3202 | 0.3304 | 0.3165 | 0.2929 |
| | Proposed | – | 0.6827 | 0.6300 | 0.6385 | 0.6167 |
| Enhancement | Random | 0.3175 | 0.4528 | 0.4533 | 0.3395 | 0.3552 |
| | Proposed | 0.8500 | 0.9083 | 0.9258 | 0.8717 | 0.8859 |
| Cyst | Random | 0.5784 | 0.5562 | 0.5584 | 0.5633 | 0.5397 |
| | Proposed | 0.7615 | 0.7807 | 0.7879 | 0.7664 | 0.7607 |
| Mass | Random | 0.3870 | 0.4529 | 0.4613 | 0.4044 | 0.3569 |
| | Proposed | 0.6094 | 0.8788 | 0.6718 | 0.6325 | 0.6211 |
| Tumor | Random | 0.3168 | 0.4829 | 0.4916 | 0.3929 | 0.3510 |
| | Proposed | 0.7063 | 0.9620 | 0.7344 | 0.7460 | 0.7400 |
| Size | Random | – | – | – | – | – |
| | Proposed | – | – | – | – | 0.9959 |

5.3. Report Generation Results

Table 3 presents the average performance of our report generation model across 5-fold cross-validation, evaluated using standard natural language generation (NLG) metrics. The model achieved a mean BLEU-4 score of 29.58, indicating moderate n-gram overlap with ground-truth sentences. ROUGE scores were also consistent, with ROUGE-1 at 28.31, ROUGE-2 at 9.59, and ROUGE-L at 21.99, reflecting reasonable lexical and structural alignment between the generated and reference sentences.

These results suggest that the model is capable of generating radiology sentences that are both clinically coherent and semantically relevant. However, the relatively

low ROUGE-2 score indicates that bigram-level fluency and specificity remain limited—likely due to variability in radiology writing styles and the limited size of the training corpus. Incorporating domain-specific pretraining or reinforcement learning with clinical feedback may further improve factual accuracy and linguistic fidelity in future work.

Table 3: Performance of report generation

| Metric | BLEU-4 | ROUGE-1 | ROUGE-2 | ROUGE-L |
|------------|--------|---------|---------|---------|
| Mean Value | 29.58 | 28.31 | 9.59 | 21.99 |

6. Limitations

Data Imbalance and Dataset Size. Our dataset is relatively small and exhibits substantial class imbalance, particularly for rare feature labels such as *endophytic* and *tumor*. For example, the seemingly perfect performance reported for the *Exophytic* category is due to a single minority instance appearing in both the training and validation sets, resulting in inflated metrics. Expanding the dataset and improving class balance will be essential for obtaining more reliable performance estimates [9, 10].

Incomplete Annotations from Reports. All feature labels were extracted from narrative radiology reports, which frequently omit attributes that are not considered clinically significant. As a result, certain features—such as *enhancement* and *attenuation*—contain a large proportion of “unknown” values. Although we intentionally preserved these missing entries to reflect real-world reporting practices, they introduce challenges in both model training and evaluation.

2D Slice Limitation. Our current pipeline operates on individual 2D CT slices. While this design simplifies preprocessing and alignment with sentence-level annotations, it limits the model’s capacity to capture spatial continuity. Many renal lesions span multiple slices, and extending the framework to volumetric (3D) modeling could improve performance by leveraging richer spatial context.

Limitations of Text-Based Evaluation. The reference sentences used for evaluating report generation were extracted from clinician-written reports that vary in style, wording, and completeness. Traditional NLG metrics such as BLEU and ROUGE are limited in their ability to assess clinical accuracy.

7. Conclusion

This study presents a clinically grounded framework for generating renal radiology reports from 2D CT slices, combining structured abnormality detection with multimodal report generation. Our approach mirrors key steps in the radiology workflow and demonstrates the feasibility of integrating feature-aware modeling with large vision-language models in a modular and interpretable manner.

While the current system is limited to 2D slices, it lays the groundwork for more comprehensive and clinically realistic solutions. In future work, we plan to extend the framework to full 3D CT volumes to capture richer anatomical context and enable more robust report generation. Such advancements may further support clinical decision-making in renal cancer diagnosis and management.

References

- [1] Luigi Cirillo, Samantha Innocenti, and Francesca Becherucci. Global epidemiology of kidney cancer. *Nephrology Dialysis Transplantation*, 39(6):920–928, 2024.
- [2] Rebecca L. Siegel, Kimberly D. Miller, Nivedita S. Wagle, and Ahmedin Jemal. Cancer statistics, 2024. *CA: A Cancer Journal for Clinicians*, 74(1):7–33, 2024.
- [3] Sandeep Anand Padala, Adam Barsouk, Krishna Chaitanya Thandra, Kalyan Saginala, Azeem Mohammed, Anusha Vakiti, Prashanth Rawla, and Alexander Barsouk. Epidemiology of renal cell carcinoma. *World journal of oncology*, 11(3):79, 2020.
- [4] Karan Singhal, Shekoofeh Azizi, Tao Tu, S Sara Mahdavi, Jason Wei, Hyung Won Chung, Nathan Scales, Ajay Tanwani, Heather Cole-Lewis, Stephen Pfohl, et al. Large language models encode clinical knowledge. *Nature*, 620(7972):172–180, 2023.
- [5] Peter Lee, Sebastien Bubeck, and Joseph Petro. Benefits, limits, and risks of gpt-4 as an ai chatbot for medicine. *New England Journal of Medicine*, 388(13):1233–1239, 2023.
- [6] Ce Zhou, Qian Li, Chen Li, Jun Yu, Yixin Liu, Guangjing Wang, Kai Zhang, Cheng Ji, Qiben Yan, Lifang He, et al. A comprehensive survey on pretrained foundation models: A history from bert to chatgpt. *International Journal of Machine Learning and Cybernetics*, pages 1–65, 2024.
- [7] Lei Huang, Weijiang Yu, Weitao Ma, Weihong Zhong, Zhangyin Feng, Haotian Wang, Qianglong Chen, Weihua Peng, Xiaocheng Feng, Bing Qin, et al. A survey on hallucination in large language models: Principles, taxonomy, challenges, and open questions. *ACM Transactions on Information Systems*, 43(2):1–55, 2025.

- [8] Haotian Liu, Chunyuan Li, Qingyang Wu, and Yong Jae Lee. Visual instruction tuning. *Advances in neural information processing systems*, 36:34892–34916, 2023.
- [9] Alistair EW Johnson, Tom J Pollard, Seth J Berkowitz, Nathaniel R Greenbaum, Matthew P Lungren, Chih-ying Deng, Roger G Mark, and Steven Horng. Mimic-cxr, a de-identified publicly available database of chest radiographs with free-text reports. *Scientific data*, 6(1):317, 2019.
- [10] Jeremy Irvin, Pranav Rajpurkar, Michael Ko, Yifan Yu, Silvana Ciurea-Ilcus, Chris Chute, Henrik Marklund, Behzad Haghgoo, Robyn Ball, Katie Shpanskaya, et al. Chexpert: A large chest radiograph dataset with uncertainty labels and expert comparison. In *Proceedings of the AAAI conference on artificial intelligence*, volume 33, pages 590–597, 2019.
- [11] Navdeep Kaur, Ajay Mittal, and Gurpreem Singh. Methods for automatic generation of radiological reports of chest radiographs: a comprehensive survey. *Multimedia Tools and Applications*, 81(10):13409–13439, 2022.
- [12] Dalia Alzu’bi, Malak Abdullah, Ismail Hmeidi, Rami AlAzab, Maha Gharaibeh, Mwaffaq El-Heis, Khaled H Almotairi, Agostino Forestiero, Ahmad MohdAziz Hussein, and Laith Abualigah. Kidney tumor detection and classification based on deep learning approaches: a new dataset in ct scans. *Journal of Healthcare Engineering*, 2022(1):3861161, 2022.
- [13] Md Nazmul Islam, Mehedi Hasan, Md Kabir Hossain, Md Golam Rabiul Alam, Md Zia Uddin, and Ahmet Soylu. Vision transformer and explainable transfer learning models for auto detection of kidney cyst, stone and tumor from ct-radiography. *Scientific Reports*, 12(1):11440, 2022.
- [14] Kwang-Hyun Uhm, Seung-Won Jung, Moon Hyung Choi, Hong-Kyu Shin, Jae-Ik Yoo, Se Won Oh, Jee Young Kim, Hyun Gi Kim, Young Joon Lee, Seo Yeon Youn, et al. Deep learning for end-to-end kidney cancer diagnosis on multi-phase abdominal computed tomography. *NPJ precision oncology*, 5(1):54, 2021.
- [15] Kadir Yildirim, Pinar Gundogan Bozdog, Muhammed Talo, Ozal Yildirim, Murat Karabatak, and U Rajendra Acharya. Deep learning model for automated kidney stone detection using coronal ct images. *Computers in biology and medicine*, 135:104569, 2021.
- [16] Makoto Nishino, Maiko Fujimori, Takafumi Koyama, Makoto Hirata, Noriko Tanabe, Toshio Shimizu, Noboru Yamamoto, and Yosuke Uchitomi. Prevalence of psychological distress, quality of life, and satisfaction among patients and family members following comprehensive genomic profiling testing: protocol of the quality of life for cancer genomics and advanced therapeutics (q-cat) study. *Plos one*, 18(5):e0283968, 2023.

- [17] Harsha Nori, Nicholas King, Scott Mayer McKinney, Dean Carignan, and Eric Horvitz. Capabilities of gpt-4 on medical challenge problems. *arXiv preprint arXiv:2303.13375*, 2023.
- [18] Karan Singhal, Tao Tu, Juraj Gottweis, Rory Sayres, Ellery Wulczyn, Mohamed Amin, Le Hou, Kevin Clark, Stephen R Pfohl, Heather Cole-Lewis, et al. Toward expert-level medical question answering with large language models. *Nature Medicine*, pages 1–8, 2025.
- [19] Jinze Bai, Shuai Bai, Yunfei Chu, Zeyu Cui, Kai Dang, Xiaodong Deng, Yang Fan, Wenbin Ge, Yu Han, Fei Huang, et al. Qwen technical report. *arXiv preprint arXiv:2309.16609*, 2023.
- [20] Renqian Luo, Liai Sun, Yingce Xia, Tao Qin, Sheng Zhang, Hoifung Poon, and Tie-Yan Liu. Biogpt: generative pre-trained transformer for biomedical text generation and mining. *Briefings in bioinformatics*, 23(6):bbac409, 2022.
- [21] Chaoyi Wu, Weixiong Lin, Xiaoman Zhang, Ya Zhang, Weidi Xie, and Yanfeng Wang. Pmc-llama: toward building open-source language models for medicine. *Journal of the American Medical Informatics Association*, 31(9):1833–1843, 2024.
- [22] Dina Demner-Fushman, Marc D Kohli, Marc B Rosenman, Sonya E Shooshan, Laritza Rodriguez, Sameer Antani, George R Thoma, and Clement J McDonald. Preparing a collection of radiology examinations for distribution and retrieval. *Journal of the American Medical Informatics Association*, 23(2):304–310, 2016.
- [23] Ibrahim Ethem Hamamci, Sezgin Er, Chenyu Wang, Furkan Almas, Ayse Gulnihhan Simsek, Sevval Nil Esirgun, Irem Doga, Omer Faruk Durugol, Weicheng Dai, Murong Xu, et al. Developing generalist foundation models from a multimodal dataset for 3d computed tomography. *arXiv preprint arXiv:2403.17834*, 2024.
- [24] Jiayu Lei, Xiaoman Zhang, Chaoyi Wu, Lisong Dai, Ya Zhang, Yanyong Zhang, Yanfeng Wang, Weidi Xie, and Yuehua Li. Autorg-brain: Grounded report generation for brain mri. *arXiv preprint arXiv:2407.16684*, 2024.
- [25] Hyeon Seok Choi, Jun Yeong Song, Kyung Hwan Shin, Ji Hyun Chang, and Bum-Sup Jang. Developing prompts from large language model for extracting clinical information from pathology and ultrasound reports in breast cancer. *Radiation oncology journal*, 41(3):209, 2023.
- [26] Rinze Reinhard, Mandy van der Zon-Conijn, and Robin Smithuis. Solid renal masses, 2016.

- [27] Smith Andrew. Standardized report template for initial renal mass characterization by renal ct without and with intravenous contrast, 2021.
- [28] Konstantinos Sechidis, Grigorios Tsoumakas, and Ioannis Vlahavas. On the stratification of multi-label data. In *Machine Learning and Knowledge Discovery in Databases: European Conference, ECML PKDD 2011, Athens, Greece, September 5-9, 2011, Proceedings, Part III 22*, pages 145–158. Springer, 2011.
- [29] Piotr Szymański and Tomasz Kajdanowicz. A network perspective on stratification of multi-label data. In *First International Workshop on Learning with Imbalanced Domains: Theory and Applications*, pages 22–35. PMLR, 2017.
- [30] Kaiming He, Xiangyu Zhang, Shaoqing Ren, and Jian Sun. Deep residual learning for image recognition. *Proceedings of the IEEE conference on computer vision and pattern recognition*, pages 770–778, 2016.
- [31] Guansong Pang, Chunhua Shen, Longbing Cao, and Anton Van Den Hengel. Deep learning for anomaly detection: A review. *ACM computing surveys (CSUR)*, 54(2):1–38, 2021.
- [32] Yaowei Zheng, Richong Zhang, Junhao Zhang, Yanhan Ye, Zheyang Luo, Zhangchi Feng, and Yongqiang Ma. Llamafactory: Unified efficient fine-tuning of 100+ language models. *arXiv preprint arXiv:2403.13372*, 2024.
- [33] Kishore Papineni, Salim Roukos, Todd Ward, and Wei-Jing Zhu. Bleu: a method for automatic evaluation of machine translation. In *Proceedings of the 40th annual meeting on association for computational linguistics*, pages 311–318. Association for Computational Linguistics, 2002.
- [34] Chin-Yew Lin. Rouge: A package for automatic evaluation of summaries. In *Proceedings of the ACL workshop on Text Summarization Branches Out*, pages 74–81, 2004.

Appendix A. Prompt Design

We designed a series of prompts to guide large language models in three key components of our pipeline. First, sentence-level filtering was performed using LLM to identify renal-related content that references specific CT slices. Second, structured abnormality features were extracted from the filtered sentences, focusing on lesion characteristics relevant to renal cancer. Third, we fine-tuned the Qwen-VL 2.5 vision-language model for report generation, using paired inputs of CT slices and extracted features. All prompts are provided below in their original form.

Prompt 1: Renal Sentence Extraction

Task: Identify and extract kidney/renal-related text snippets from a radiology CT report while excluding adrenal-related content.

1. Analyze the Report Structure: Common sections include:

- HISTORY
- EXAM
- PRIOR STUDY
- FINDINGS
- (Other possible sections)

2. Identify Renal-Relevant Terms:

- *Include:* kidney, renal, nephro-, ureter, cyst, calculi, stone, hydronephrosis, parenchyma, cortex, medulla, atrophy, mass, tumor, lesion
- *Exclude:* adrenal-related terms (e.g., adrenal, suprarenal)

3. Extract and Format Results: For each section, output:

- Direct quotes of renal-relevant snippets, or
- "none" if no renal terms are found

Output Template:

```
{
  "renal_extracts": {
    "HISTORY": extracted snippet or "none",
    "EXAM": extracted snippet or "none",
    "PRIOR STUDY": extracted snippet or "none",
    "FINDINGS": extracted snippet or "none"
  }
}
```

Prompt 2: Renal Feature Extraction

Task: Identify and extract kidney/renal-related abnormality information from a radiology CT report. Focus on lesions, masses, cysts, and tumors; exclude kidney stones and hydronephrosis.

Instructions:

- Detect all relevant abnormalities (lesion, mass, cyst, tumor).
- If no abnormality is found, return "Abnormality": `false`.
- Otherwise, return "Abnormality": `true` with extracted fields.

Fields to Extract:

- **Location:** Position (left/right)
- **Size:** Raw size string and standardized size in cm
- **Characteristics:** Exophytic, attenuation, enhancement
- **Classification:** Boolean flags for Lesion, Cyst, Mass, Tumor
- **Raw Fields:** Verbatim report text (prefixed with `Raw_`)

Missing Values: Use "unknown" for any unspecified field.

Example Output Format:

```
{
  "Abnormality": true,
  "Abnormality_Info": [
    {
      "Position": "left",
      "Raw_Size": "3.2 * 2.8 cm",
      "Size_cm": 3.2,
      "Exophytic": "exophytic",
      "Attenuation": "Hyperattenuating",
      "Enhancement": "enhancement",
      "Lesion": true,
      "Cyst": true,
      "Mass": true,
      "Tumor": false,
    },
  ],
}
```

Classification Rules: Use domain-informed heuristics such as:

- "denser than water" → Hyperattenuating
- "complex cystic mass" → Cyst: true, Mass: true
- Any mention suggestive of RCC (e.g., "suspicious for RCC") → Tumor: true

Prompt 3: Report Generation

System Prompt: This system generates CT radiology reports specifically for the diagnosis of renal abnormalities (lesion, cyst, mass, tumor).

User Input: You will be provided with a renal CT slice image and a set of imaging features. Analyze the image based on the given features and generate a comprehensive radiology report.

Features:

- Position: `left`
- Largest size for the lesion (cm): `1.78`
- Exophytic: `exophytic`
- Attenuation: `hypoattenuating`
- Enhancement: `enhancement`
- Cyst: `true`
- Mass: `false`
- Tumor: `false`

Image (CT scan slice): `<image>`

Expected Output:

Left kidney: There is a 3.6 x 3.4 x 2.9 cm exophytic, complex cystic and solid mass with focal punctate calcification identified at the superior pole of the left kidney. This mass extends into the left quadratus lumborum muscle with loss of fat planes of separation.

Appendix B. Label Distribution

Table B.4 summarizes the distribution of renal feature labels in one representative fold of our 5-fold cross-validation setup. It reflects the class balance and prevalence of missing values that our stratified sampling strategy aimed to preserve.

Table B.4: Label Distribution in One Fold of the Cross-Validation Dataset

| Attribute | Training | Validation |
|-------------------------|------------------|-------------------|
| Position | | |
| Right kidney | 58 | 10 |
| Left kidney | 46 | 15 |
| Unknown | 1 | 0 |
| Lesion Size (cm) | | |
| Mean \pm SD | 1.73 \pm 1.26 | 1.61 \pm 0.95 |
| Max / Min / Median | 7.4 / 0.28 / 1.4 | 3.6 / 0.5 / 1.4 |
| Unknown | 14 | 4 |
| Growth Pattern | | |
| Exophytic | 20 | 6 |
| Endophytic | 1 | 1 |
| Unknown | 84 | 18 |
| Attenuation | | |
| Hypoattenuating | 34 | 9 |
| Hyperattenuating | 25 | 5 |
| Isoattenuating | 4 | 2 |
| Unknown | 42 | 9 |
| Enhancement | | |
| Enhancement | 22 | 4 |
| Non-enhancement | 8 | 2 |
| Unknown | 75 | 19 |
| Cyst | | |
| Present | 62 | 16 |
| Absent | 43 | 9 |
| Mass | | |
| Present | 11 | 4 |
| Absent | 94 | 21 |
| Tumor | | |
| Present | 6 | 1 |
| Absent | 99 | 24 |